AGGREGATION-FREE FATIGUE CONSTRAINED TOPOLOGY OPTIMIZATION USING THE CONSTRAINED NATURAL ELEMENT METHOD

Yanda Chen[1], **Eric Monteiro**[1], **Imade Koutiri**[1], **Véronique Favier**[1]

Laboratoire PIMM, Arts et Metiers Institute of Technology, CNRS, CNAM, HESAM Universite, 151 boulevard de l'Hopital, 75013 Paris
e-mail: {yanda.chen,eric.monteiro,imade.koutiri,veronique.favier}@ensam.eu

Keywords: Topology Optimization, Fatigue Constraint, Constrained Natural Element Method, Augmented Lagrangian Method.

Abstract. *Fatigue resistance is one of the most important design criteria to ensure the safety of mechanical structures. In this paper, a topology optimization methodology for volume minimization under local fatigue constraints based on the augmented Lagrangian method and the constrained natural element method is proposed. The Sines fatigue criteria is used to define the equivalent alternating and average stresses to address fatigue resistance of additive manufactured Ti-6Al-4V alloy structure for infinite life. Since the fatigue criteria under consideration is based on stress invariants, the fatigue-driven problem has the same difficulties as the stress-based topology optimization problem, so that similar strategies can be used to circumvent the problem of stress singularity and the need for a large number of evaluation points. Although a large number of constraints are required to maintain the local nature of stress, the formulation presented requires only one adjoint vector, which leads to an efficient sensitivity assessment. Several numerical examples are presented to demonstrate the effectiveness of the proposed method.*

1 INTRODUCTION

Topology optimization (TO) aims at determining the optimal material distribution within the design domain for a given set of boundary conditions. On one hand, the physical problems can be solved by numerical methods like the finite element method (FEM) or meshless methods. On the other hand, the optimization can be completed by mathematical programming techniques such as the method of moving asymptotes (MMA) or the method based on the augmented Lagrangian (AL) formula. Several TO approaches have been proposed since the pioneer work by Bendsøe and Kikuchi in 1988 [1], namely density-based method, level set-based method, homogenization method and evolutionary structural optimization method. The comparison and critical review of the above methods have been given in detail by Sigmund and Maute [2].

Typically, designs generated by TO often include free-form and complex shapes that are complicated or cannot be manufactured using traditional production methods. However, TO designs are well suited for additive manufacturing processes that have more relaxed design rules and can easily replicate complex shapes without additional cost. Additive manufactured materials and components for critical load-bearing applications are usually subjected to cyclic loading and fatigue failure is a major consideration in their design. In addition, due to the multi-axial nature of the loads and complex geometries manufactured by additive manufacturing, it is necessary to take multi-axial fatigue into account in TO. Fatigue constrained TO aims to reduce the overall mass by finding the (local) optimal material distribution that satisfies the specific fatigue criteria for a given set of cyclic loads.

TO was first formulated as minimizing the strain energy, i.e., the compliance that obeys the volume constraint. The elaboration of this concept led to the application to a variety of static responses, dynamic responses and even multiphysics system responses. However, these designs ignore material strength limitations and still require manual adjustments or shape optimization to enable the structure to withstand the applied loads. In order to produce structural components that meet specific functional requirements, structural failure must be prevented at every point of the component, for example, by developing specific topology optimization schemes that allow the design to meet a given stress-based requirement and even maintain the life of the structure during a given number of load cycles. The main issues encountered in stress and fatigue based topology optimization are the singularity phenomenon and the large-scale optimization problem caused by the local behavior of stresses.

Several static and quasi-static fatigue models have been developed for topology optimization of linear elastic structures, thereby avoiding the high computational cost when facing a large number of loading sequences. Sherif et al. [3] addressed the dynamic property of load conditions in TO by applying equivalent static loads. The work by Holmberg et al. [4] introduced the fatigue constrained TO based on probability, where the critical fatigue state was determined as the maximum stress level exceeding the allowable cumulative damage. Jeong et al. [5] developed the TO method with dynamic fatigue and static failure constraints under proportional loads. Lee et al. [6] assessed a TO method subjected to fatigue failure in the frequency domain for random load. Collet et al. [7] proposed an optimization tool for lightweight design accompanied by compliance and fatigue constraints through a modified Goodman failure criteria based on the Sines theory. Using the Palmgren-Miner's linear damage rule, S-N curves and Sines fatigue criteria, Oest and Lund [8] investigated TO under finite-life fatigue constraints. Zhang et al. [9] performed fatigue-based TO under non-proportional loading. Suresh et al. [10] proposed a fatigue constrained TO formulation based on continuous-time approach to consider

general load histories including non-proportional loads. Chen et al. [11] considered the fatigue constrained TO with cumulative fatigue damage and discussed the influence of damage penalization parameters and load parameters on the final design. In addition to the SIMP method used in the above studies, the fatigue-constrained TO problem has also been solved by the evolutionary structural optimization method (Nabaki et al. [12]). The similarities of the above studies lie in the use of FEM to solve the equilibrium equation and employ aggregation technology or active set strategy to reduce the number of constraints.

The most widely employed Lagrangian-type finite elements suffer from numerical instabilities, such as checkerboard pathology and single-node connections (Diaz and Sigmund [13]). A feasible alternative is to use polygonal finite elements to suppress checkerboard patterns and reduce mesh dependence (Talischi et al. [14]- [16]). However, due to technical difficulties, there are no reliable processors available to create high-quality polytopal meshes for 3D complex geometries, which limits their application to TO over complex design domains. To overcome the mesh dependency, several meshless methods have been applied in conventional compliance-based TO problems (Li and Atluri [17]; Luo et al. [18]; Shobeiri [19]) and they have recently started to be applied to TO problems based on stress constraints (Ullah et al. [20]). The major drawback of the commonly used meshless method, such as Element-free Galerkin Method, is the way to impose the essential boundary conditions since the interpolation function does not satisfy the Kronecker delta property. To address this problem, Chen et al. [21] applied the constrained natural element method (CNEM) in tandem with solid isotropic material with penalization method (SIMP) to TO problems. In addition, aggregation technology reduces the computational cost at the expense of losing control over the local behavior and lead to highly nonlinear which makes the solution become unstable and parameter dependent. The disadvantage of the active set approach lie in the active set may still become relatively large during optimization, since the stresses in the optimized design are usually uniformly distributed, leading to a large number of elements approaching the stress limit.

In this paper, the method based on CNEM and SIMP is applied to deal with a class of TO problems with fatigue constraints under sinusoidal cyclic loading. Furthermore, a scheme based on the AL method is adopted, which deals with the TO problem according to the local definition of stress without using the constraint aggregation technique. Since the given formula requires only one adjoint vector, this leads to an efficient sensitivity analysis. Several TO results with Sines fatigue criteria constraints are provided. The reminder of the paper is organized as follows. Section 2 introduces the construction of interpolation function and the calculation of numerical integration of CNEM. Section 3 presents the fatigue constrained TO formula of continuum structures and the implementation of AL. Then, several numerical examples are shown in Section 4. Finally, section 5 gives the concluding comments of this paper.

2 The Constrained Natural Element Method

The natural element method (NEM) is an efficient numerical method which was proposed by Braun and Sambridge [22] to solve partial differential equations along with highly irregular meshes. Sukumar et al. [23] has shown that the interpolation between adjacent nodes along any convex boundary in NEM is strictly linear, which facilitates the application of essential boundary conditions. However, on non-convex boundaries, they may be influenced by the nodes located in the domain or over the non-convex boundary far from the node under consideration. To address this phenomenon, Yvonnet et al. [24] proposed the CNEM, which introduced the visibility criteria in NEM to restrict the natural neighborhood relations of the selected node pairs to construct the interpolation function in 2D. On this basis, Illoul and Lorong [25] extended its

application to 3D.

2.1 Constrained Voronoi Diagram

In the NEM, the Voronoi diagram of a cloud of nodes, shown in Fig. 1, divides the bounded domain Ω^D in D-dimensions into a group of Voronoi cells $\mathcal{V}_i$, such that any point M within $\mathcal{V}_i$ is closer to node i than any other node $j (j \neq i)$:

$$\mathcal{V}_i = \left\{ M \in \Omega^D : d\left(\boldsymbol{x}, \boldsymbol{x}_i\right) \leq d\left(\boldsymbol{x}, \boldsymbol{x}_j\right) \forall j \neq i \right\} \tag{1}$$

where $\boldsymbol{x}$ and $\boldsymbol{x}_i$ represent the coordinates of point M and node i respectively while $d\left(\boldsymbol{x}, \boldsymbol{x}_j\right)$ is the Euclidean distance between point M and node j. According to this definition, if a line segment connecting two neighbors crosses the domain boundary Γ, then node i influences node j, which is incorrect, see Fig. 2. To overcome this issue, a visibility criteria is introduced in the definition of Voronoi diagram to give rise to the constrained Voronoi diagram:

$$\mathcal{V}_i^C = \left\{ M \in \Omega^D : d\left(\boldsymbol{x}, \boldsymbol{x}_i\right) \leq d\left(\boldsymbol{x}, \boldsymbol{x}_j\right) \forall j \neq i \cap x \text{ is visible from } i \text{ and } j \right\} \tag{2}$$

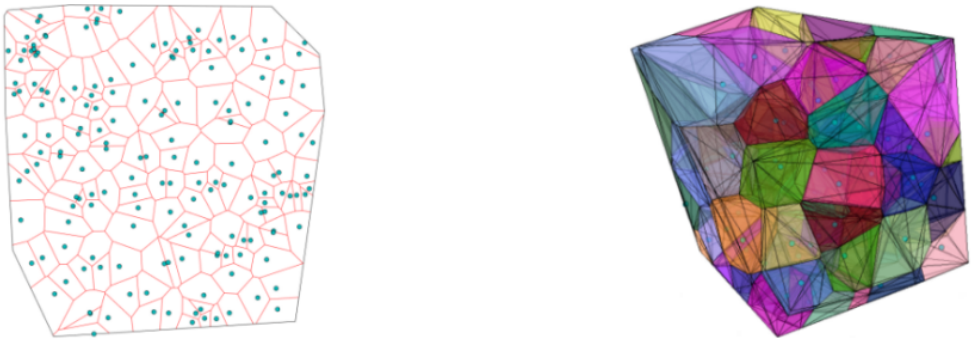

Figure 1: Voronoi diagram of a cloud of N nodes in 2D (left) and 3D (right)

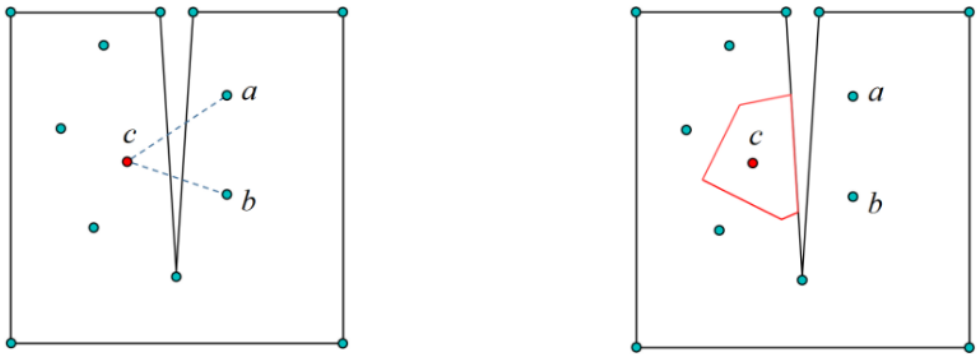

Figure 2: Visibility criterion (left) and constrained Voronoi cell of node c (right)

2.2 Construction of the Interpolation Function

There exist different interpolation procedures based upon natural neighborhoods for CNEM. The Sibson interpolant [26] is one of the most widely used and its construction in 2D is shown in Fig. 3. First, the original constrained Voronoi diagram is modified locally by introducing a new Voronoi cell attached to point $\boldsymbol{x}$ (blue area). Then, the interpolation function is computed based on the geometrical considerations:

$$\phi_i(\boldsymbol{x}) = \frac{V_i(\boldsymbol{x})}{V(\boldsymbol{x})} \text{ with } V(\boldsymbol{x}) = \sum_{j=1}^{n} V_j(\boldsymbol{x}) \tag{3}$$

where $V_i(\boldsymbol{x})$ is the Lebesgue measure of the intersection (green area) of Voronoi cell $\mathcal{V}_i^C$ (yellow area) and the new Voronoi cell $\mathcal{V}_x^C$ (blue area), $V(\boldsymbol{x})$ represents the Lebesgue measure of the new Voronoi cell $\mathcal{V}_x^C$ and n is the number of natural neighbors of point $\boldsymbol{x}$. Unlike the FEM and other meshless methods, the construction of interpolation functions in CNEM is purely geometric, which does not involve user-defined parameters. Sibson interpolant satisfies the Kronecker delta property, the partition of unity property and the linear consistency [23]:

$$\phi_i\left(\boldsymbol{x}_j\right) = \delta_{ij}, \quad \sum_{i=1}^{n} \phi_i(\boldsymbol{x}) = 1, \quad u(\boldsymbol{x}) = \sum_{i=1}^{n} \phi_i(\boldsymbol{x})\, u_i \tag{4}$$

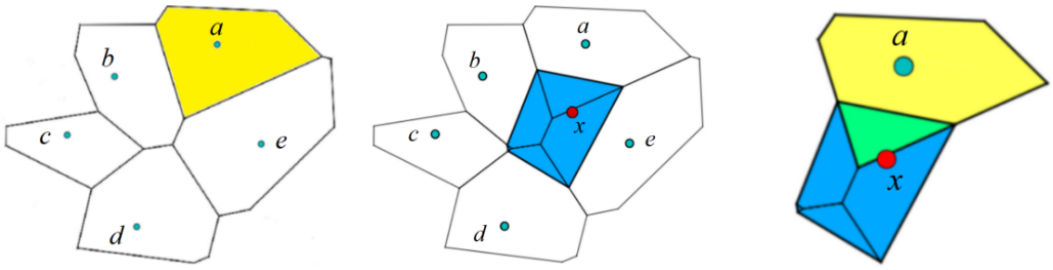

Figure 3: Process to compute Sibson interpolant in 2D

2.3 Discrete Weak Form

The governing equation of equilibrium of a linear elastic body Ω can be expressed as:

$$\nabla^T \boldsymbol{\sigma} + \boldsymbol{b} = \boldsymbol{0} \tag{5}$$

subjected to the boundary conditions:

$$\begin{aligned} \boldsymbol{\sigma n} &= \overline{\boldsymbol{t}} \\ \boldsymbol{u} &= \overline{\boldsymbol{u}} \end{aligned} \tag{6}$$

where $\boldsymbol{\sigma}$ and $\boldsymbol{b}$ are the stress tensor and body force vector respectively, $\overline{\boldsymbol{t}}$ stands for the prescribed traction vector on the Von Neumann boundary Γ_t and $\overline{\boldsymbol{u}}$ represents the prescribed displacement

vector over the Dirichlet boundary Γ_u, $\boldsymbol{n}$ is the outer normal unit vector to the boundary $\Gamma = \Gamma_t \cup \Gamma_u$. Introducing any arbitrary function $\boldsymbol{\delta u}$, the associated weak form yields to:

$$\int_{\Omega} \boldsymbol{\delta \varepsilon}^T \boldsymbol{\sigma} d\Omega - \int_{\Omega} \boldsymbol{\delta u}^T \boldsymbol{b} d\Omega - \int_{\Gamma_t} \boldsymbol{\delta u}^{\boldsymbol{T}} \, \bar{\boldsymbol{t}} \, d\Gamma = 0 \tag{7}$$

In order to obtain the CNEM discrete weak form, the design domain Ω is represented by appropriately distributed nodes and the corresponding constrained Voronoi diagram. Then, using Eq. 3, the displacement at any position $\boldsymbol{x}$ can be expressed by:

$$\boldsymbol{u}^h(\boldsymbol{x}) = \sum_{i=1}^{n} \boldsymbol{\Phi}_i(\boldsymbol{x}) \boldsymbol{u}_i \tag{8}$$

where $\boldsymbol{\Phi}_i$ and $\boldsymbol{u}_i$ are the interpolation function matrix and displacement vector of node i respectively. The strain vector $\boldsymbol{\varepsilon}^h$ at position $\boldsymbol{x}$ reads:

$$\boldsymbol{\varepsilon}^h(\boldsymbol{x}) = \boldsymbol{L} \boldsymbol{u}^h(\boldsymbol{x}) = \sum_{i=1}^{n} \boldsymbol{B}_i(\boldsymbol{x}) \boldsymbol{u}_i \tag{9}$$

where $\boldsymbol{L}$ is the differential operator matrix and $\boldsymbol{B}_i$ represents the strain-displacement matrix of node i. Finally, using the constitutive equation, the stress tensor $\boldsymbol{\sigma}^h$ can be obtained by:

$$\boldsymbol{\sigma}^h(\boldsymbol{x}) = \sum_{i=1}^{n} \boldsymbol{C} \boldsymbol{B}_i(\boldsymbol{x}) \boldsymbol{u}_i \tag{10}$$

where $\boldsymbol{C}$ is the material constitutive matrix. Substituting Eqs. 8, 9 and 10 into Eq. 7, the discrete weak form reads:

$$\sum_{j=1}^{N} \sum_{i=1}^{N} \boldsymbol{\delta u}_j^T \left(\int_{\Omega} \boldsymbol{B}_j^T \boldsymbol{C} \boldsymbol{B}_i \boldsymbol{d} \Omega \right) \boldsymbol{u}_i = \sum_{j=1}^{N} \boldsymbol{\delta u}_j^T \left(\int_{\Gamma_t} \boldsymbol{\Phi}_j^T \, \bar{\boldsymbol{t}} \, d\Gamma \right) \tag{11}$$

where N is the number of nodes. Using the arbitrariness of $\boldsymbol{\delta u}$, Eq. 11 yields to the following matrix system:

$$\boldsymbol{K u} = \boldsymbol{f} \tag{12}$$

where $\boldsymbol{K}$ is the global stiffness matrix while $\boldsymbol{u}$ and $\boldsymbol{f}$ are the displacement and the force vectors respectively.

The non-polynomial nature of the CNEM interpolation function leads to the use of a large number of Gauss integration points for the accurate computation of Eq. 12. To overcome this, the stabilized conforming nodal integration scheme (SCNI) proposed by Chen et al. [27] is applied in this study. In SCNI, the strain smoothing is performed to stabilize the nodal integration:

$$\boldsymbol{\varepsilon}_i(\boldsymbol{x}) = \frac{1}{V_i(\boldsymbol{x})} \int_{\Omega_i} \boldsymbol{B}_i(\boldsymbol{x}) \boldsymbol{u}_i d\Omega = \frac{1}{V_i(\boldsymbol{x})} \oint_{\Gamma_i} \boldsymbol{\Phi}_i(\boldsymbol{x}) \boldsymbol{u}_i \cdot \boldsymbol{n} d\Gamma \tag{13}$$

3 Formulation of Fatigue Constrained Topology Optimization Problem

This section is devoted to the development of a TO formulation which considers cyclic fatigue failure within the framework of the SIMP method. In industry, fatigue life is usually expressed in terms of service time, and specific parts are designed for a predetermined period of use. Therefore, there is no need to design parts for infinite life. However, the mechanical parts are designed using the so-called safe life approach such that fatigue failure will not occur during a specific finite life, or before predetermined service intervals. To perform fatigue life prediction for a given design, the high cycle fatigue life is modeled and assume that only elastic deformation occurs during cyclic loading. Inertial effects are also neglected, so that the stress state at each moment in the loading history is obtained by static linear elasticity analysis. The general optimization statement can be expressed mathematically as follows:

$$\begin{aligned} &\inf f(\boldsymbol{\rho}) = \sum_{i=1}^{N} \rho_i V_i \\ &\text{s.t.} \begin{cases} g_i(\boldsymbol{\rho}, \boldsymbol{u}) \leq 0, & i = 1, \dots m \\ 0 \leq \rho_j \leq 1, & j = 1, \dots N \end{cases} \\ &\text{with:} \qquad \boldsymbol{K}(\boldsymbol{\rho})\boldsymbol{u} = \boldsymbol{f} \end{aligned} \tag{14}$$

where $f(\boldsymbol{\rho})$ is the objective function, $\boldsymbol{\rho}$ is the vector of design variables, g_i is i-th fatigue constraint, which depends not only on the design variables, but also on the displacement, m represents the number of constraints.

3.1 Density Based Method

The direct use of design variable $\boldsymbol{\rho}$ to solve Eq. 14 does not make it a well-posed problem. In this study, the polynomial filter used by Zegard and Paulino [28] is adopted, such that $\widetilde{\boldsymbol{\rho}} = \mathcal{F}\boldsymbol{\rho}$. The (i, j)th component of filter matrix $\mathcal{F}$ is calculated as:

$$\mathcal{F}_{ij} = \frac{H_{ij}\rho_j}{\sum_{k=1}^{N} H_{ik}\rho_k}, \text{ with } H_{ij} = \max\left[0, 1 - \frac{d\left(\boldsymbol{x}_i, \boldsymbol{x}_j\right)}{R}\right]^s \tag{15}$$

where R is the radius of the filter and exponent $s \geq 1$ is the index of the filter.

The polynomial filter reduces to a conventional linear filter when $s = 1$. The advantage of using a polynomial instead of a linear function is that it reduces the influence of more distant elements and facilitates more abrupt changes in density, thereby better defining the material boundaries.

To obtain a black-and-white design without numerical instability, the so-called three field approach (Sigmund and Maute [2]) is adopted, which operates with the design variable $\boldsymbol{\rho}$, the filtered field $\widetilde{\boldsymbol{\rho}}$ and the projected field $\bar{\boldsymbol{\rho}}$. The Heaviside projection function used in this study is expressed as follows (Wang et al. [29]):

$$\bar{\rho}_i = \frac{\tanh(\beta\eta) + \tanh\left[\beta\left(\tilde{\rho}_i - \eta\right)\right]}{\tanh(\beta\eta) + \tanh[\beta(1-\eta)]} \tag{16}$$

where β controls the slope of the function near the projection threshold parameter η.

Finally, the stiffness matrix $\boldsymbol{K}$ in Eq. 14 is calculated through a typical assembly process:

$$\boldsymbol{K}(\overline{\boldsymbol{\rho}}) = \mathbb{A}_{i=1}^{N} \boldsymbol{K}_i, \text{ with } \boldsymbol{K}_i = \left[\epsilon + (1-\epsilon)\bar{\rho}_i^p\right] \boldsymbol{K}_{i0} \tag{17}$$

where $\boldsymbol{K}_i$ is the stiffness matrix of $\mathcal{V}_i^C$, $\mathbb{A}$ is an assembly operator, ϵ is the Ersatz parameter to prevent singularity, p is the penalty factor, $\boldsymbol{K}_{i0}$ is the stiffness matrix of $\mathcal{V}_i^C$ when $\bar{\rho}_i = 1$.

3.2 Multi-axial High Cycle Fatigue Criteria

Due to different dominant mechanisms, fatigue is usually heuristically classified into low cycle fatigue and high cycle fatigue. Low-cycle fatigue analysis involves loads in the range of $1 - 10^4$ cycles, while high-cycle fatigue is typically in the range of $10^4 - 10^8$ cycles. For high cycle fatigue, the stress-based fatigue criteria are widely used. Among the current stress-based multiaxial fatigue criteria, the Sines (Sines, [30]) criteria is attractive for the engineering design of high-performance fatigue components due to its ease of use. The Sines criteria is expressed as follows:

$$\sqrt{J_{2,a}^i} + \alpha_s \, \sigma_{H,\text{mean}}^i \leq \beta_s \tag{18}$$

where the parameters α_s and β_s are material parameters given by:

$$\alpha_s = 6t_{-1}/f_0 - \sqrt{3} \qquad \text{and} \qquad \beta_s = t_{-1} \tag{19}$$

where t_{-1} represents fully reversed torsion fatigue limit, f_{-1} and f_0 are the fatigue limits under fully reversed bending and repeated bending, respectively. $J_{2,a}^i$ and $\sigma_{H,\text{ mean}}^i$ represent, respectively, the amplitude of the second deviatoric stress tensor invariant over one cycle and the mean value of hydrostatic stress for node i:

$$\begin{cases} J_{2,a}^i = \boldsymbol{\sigma}_{i,a}^T \boldsymbol{M} \boldsymbol{\sigma}_{i,a} \\ \sigma_{H,\text{ mean}}^i = \frac{\sigma_{xx,\text{ mean}}^i + \sigma_{yy,\text{ mean}}^i}{3} \end{cases} \tag{20}$$

where $\boldsymbol{\sigma}_{i,a}$ is the amplitude of Cauchy stress tensor of node i during cyclic loading time T and $\sigma_{**,\text{ mean}}^i$ is the mean value of Cauchy stress component. The matrix $\boldsymbol{M}$ stands for the so-called second deviatoric stress tensor invariant matrix whose definition in 2D plane stress states:

$$\boldsymbol{M} = \begin{bmatrix} 1/3 & -1/6 & 0 \\ -1/6 & 1/3 & 0 \\ 0 & 0 & 1 \end{bmatrix} \tag{21}$$

3.3 Augmented Lagrangian Method

Instead of the popular MMA technique in the literature for fatigue constrained TO problems, an attractive approach to solve the optimization statement in Eq. 14 while satisfying the local fatigue constraint is the AL method. AL deals with local constraints by adding them to the objective function in the form of a penalty term. The solution to the constrained optimization problem is then obtained by solving a series of unconstrained optimization problems, each of which aims at minimizing the AL function $J(\overline{\boldsymbol{\rho}}, \boldsymbol{\lambda}, \mu)$. The unconstrained optimization problem in each AL iteration is expressed as follows:

$$\inf\ J^{(k)}(\overline{\boldsymbol{\rho}}) = f(\overline{\boldsymbol{\rho}}) + \frac{1}{N} P^{(k)}(\overline{\boldsymbol{\rho}}) \tag{22}$$

where the penalization term is

$$P^{(k)}(\overline{\boldsymbol{\rho}}, \boldsymbol{u}) = \sum_{j=1}^{N} \left[\lambda_j^{(k)} h_j(\overline{\boldsymbol{\rho}}, \boldsymbol{u}) + \frac{\mu^{(k)}}{2} h_j(\overline{\boldsymbol{\rho}}, \boldsymbol{u})^2 \right] \tag{23}$$

involving equality constraints

$$h_j(\overline{\boldsymbol{\rho}}, \boldsymbol{u}) = \max \left[g_j(\overline{\boldsymbol{\rho}}, \boldsymbol{u}), -\frac{\lambda_j^{(k)}}{\mu^{(k)}} \right] \tag{24}$$

where $\lambda_j^{(k)}$ is the Lagrange multiplier estimator at the k-th iteration and $\mu^{(k)} > 0$ a penalty coefficient. Both unknowns are updated at each iteration as follows (Senhora et al. [31]):

$$\mu^{(k+1)} = \min \left[\gamma \mu^{(k)}, \mu_{\max} \right] \qquad \text{and} \qquad \lambda_j^{(k+1)} = \lambda_j^{(k)} + \mu^{(k)} h_j \left(\overline{\boldsymbol{\rho}}^{(k)}, \boldsymbol{u} \right) \tag{25}$$

where $\gamma > 1$ is a constant parameter and μ_{max} is the upper limit which is used to prevent numerical instabilities. Iterations stop when both following criteria are satisfied

$$\frac{1}{N} \left| \boldsymbol{\rho}^{(k+1)} - \boldsymbol{\rho}^{(k)} \right| \leq \delta \qquad \text{and} \qquad \max \left(\sqrt{\boldsymbol{J_{2,a}}} + \alpha_s \, \boldsymbol{\sigma}_{\boldsymbol{H},\text{mean}} \right) - \beta_s \leq \delta_{\text{s}} \tag{26}$$

where δ and δ_{s} are the prescribed tolerance values for design variables and fatigue constraints, respectively. If both criteria are not satisfied, optimization terminates after a given number of iterations.

4 Numerical Results

Several numerical results are given in this section to demonstrate the performance of the proposed method. Table 1 shows the AL parameters used in this study. The mechanical and fatigue parameters of the additive manufactured Ti-6Al-4V alloy, coming from Mower and Long, [32] and Fatemi et al. [33], are listed in Table 2.

4.1 2D L-bracket

The L-bracket TO problem is one of the most widely studied problem in literature. The design domain and boundary conditions are shown in Fig. 4. The model is fully constrained at the top left edge, and a sinusoidal distributed load with an amplitude of 850N and a mean value of 0 is applied to the upper right free end along the distance $d = 6mm$. The length and thickness of this model are $L = 100mm$ and $t = 1mm$ respectively while the radius of the filter is $R = 5mm$.

First, six models involving 26001, 58201 and 103201 regular or irregular Voronoi cells, depicted in Fig. 5, are used here to check mesh sensitivity. The optimized geometries obtained by the proposed method are plotted in Fig. 5 as well as the normalized Sines fatigue constraint maps. The results are very close for the different discretization schemes: it seems that there is no mesh sensitivity. Moreover, the fatigue constraints are always locally satisfied and the von Mises stress, plotted in Fig. 6, is lower than the Yield stress everywhere.

Parameter	Description	Value
$\boldsymbol{\rho}^{(0)}$	Initial density vector	$\mathbf{0.5}$
β	Initial Heaviside projection penalization factor	1
$\beta_{\max}$	Maximum Heaviside projection penalty factor	10
η	Heaviside projection threshold	0.5
$\boldsymbol{\lambda}^{(0)}$	Initial Lagrange multiplier vector	$\mathbf{0}$
$\mu^{(0)}$	Initial penalty coefficient	10
γ	Penalty factor updating parameter	1.1
q	Nonlinear filter index	3.5
δ	Convergence tolerance of design variables for AL	0.002
δ_s	Convergence tolerance of stress constraints for AL	0.003
$MaxIter$	Maximum number of external loops	150

Table 1: Input parameters used in this study.

Parameter	Description	Value
E_0	Young's modulus	108.8 GPa
μ	Poisson's ratio	0.29
$\bar{\sigma}$	Yield stress	972 MPa
f_{-1}	Fully reversed bending fatigue limit	454 MPa
t_{-1}	Fully reversed torsional fatigue limit	300 MPa
f_0	Fully repeated bending fatigue limit	315 MPa

Table 2: Mechanical and fatigue parameters for Ti-6Al-4V alloy.

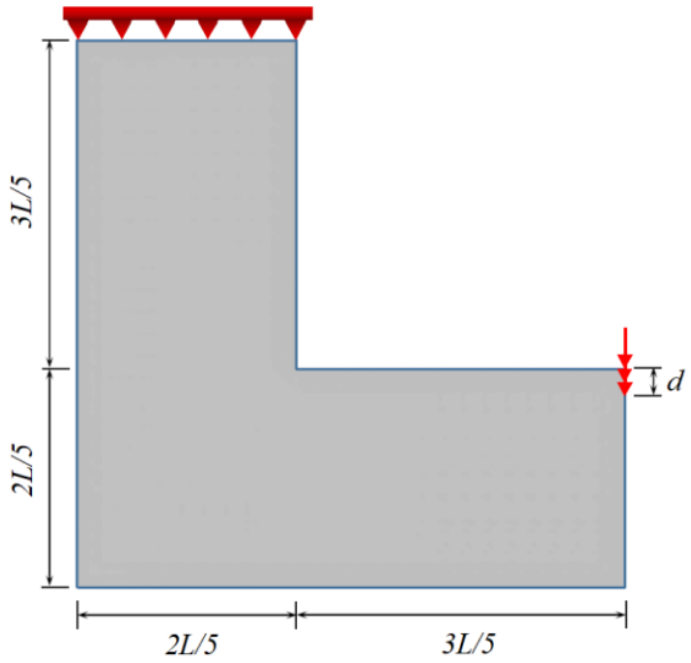

Figure 4: Design domain and boundary conditions of 2D L-bracket problem

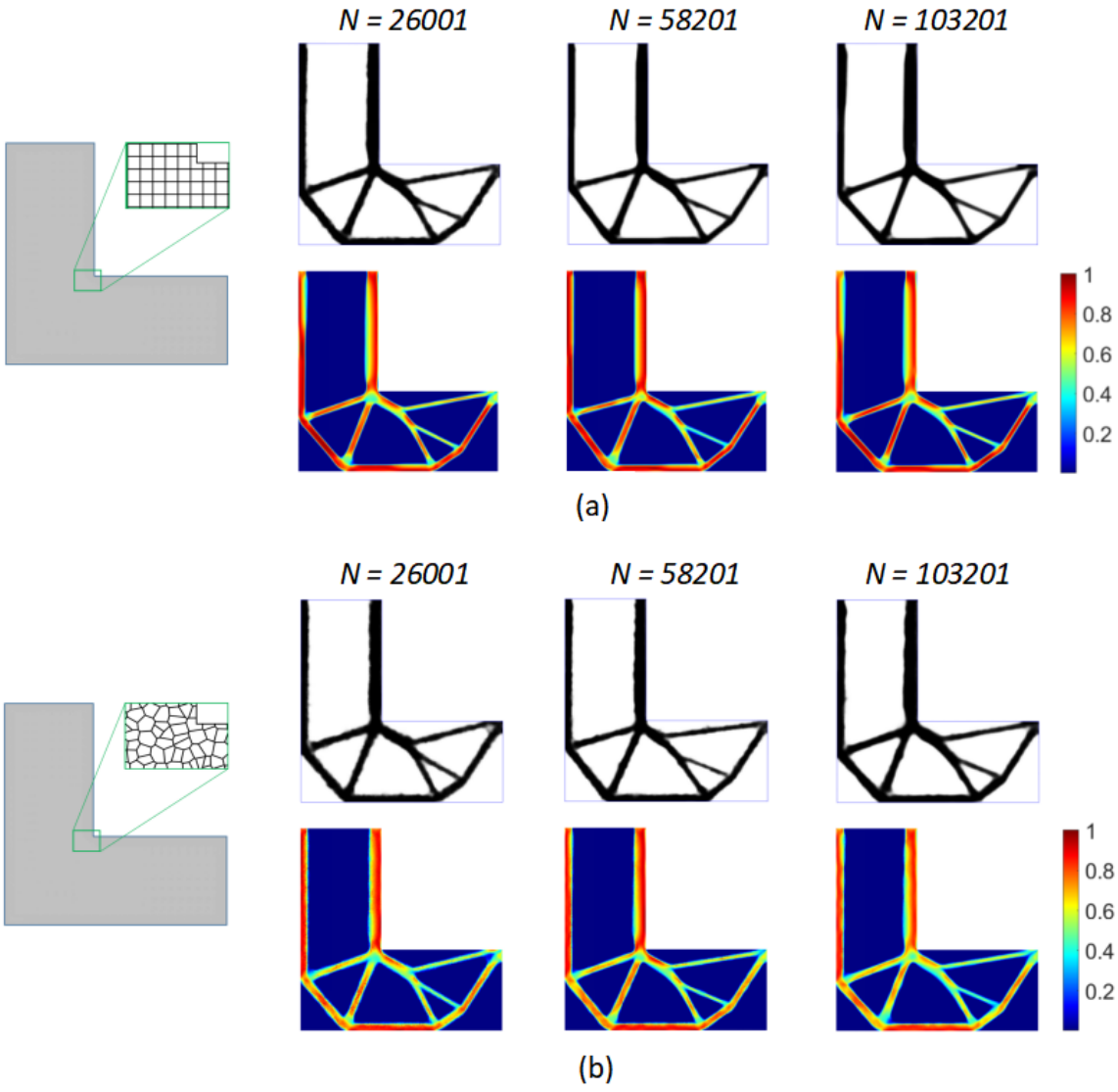

Figure 5: Sines fatigue criteria constrained TO results and normalized constraint maps under (a) regular mesh and (b) irregular mesh

4.2 2D Portal Frame

The second optimization problem is a portal frame whose geometry and boundary conditions are presented in Fig. 7. Geometrical parameters are listed in Table 3. The non convex domain is discretized using three different numbers of Voronoi cells. In order to obtain symmetric solutions, the design variables on the left and right sides are symmetrized during the optimization. Optimal geometries and normalized fatigue constraint maps depicted in Fig. 8 are obtained by using a filter radius $R = 6mm$. One can observe that there is no mesh sensitivity for the number of Voronoi cells used and that the fatigue constraints are locally satisfied. Moreover, the von Mises stress, shown in Fig. 9, is lower than the Yield stress of the material everywhere: Sines fatigue criteria seems to be more conservative than von Mises stress constraint.

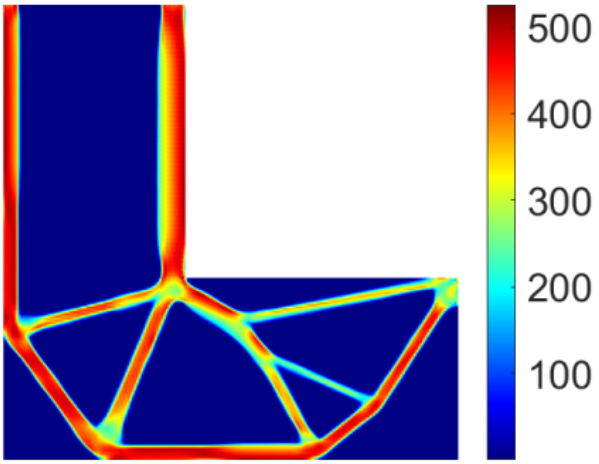

Figure 6: Von Mises stress map for 2D L-bracket problem, unit: MPa

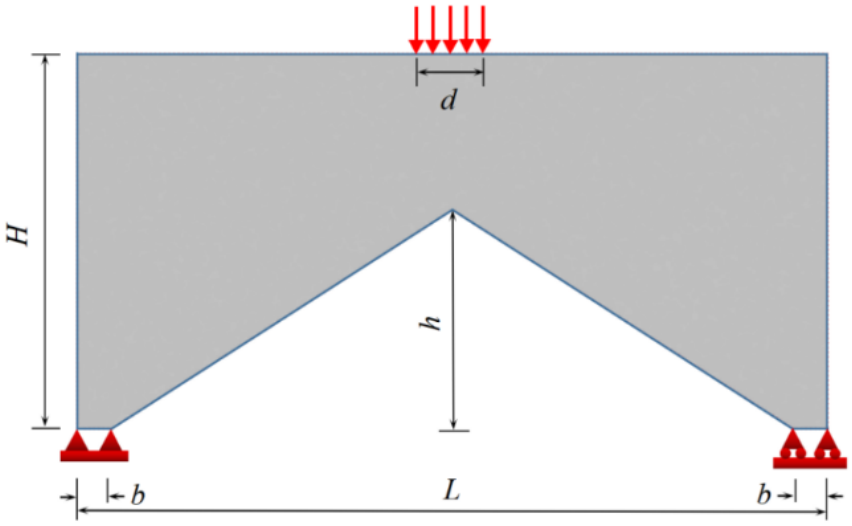

Figure 7: Design domain and boundary conditions of 2D portal frame

Parameter	Description	Value
L	Length	120 mm
H	Height	60 mm
h	Concave height	35 mm
b	Bearing length	5.5 mm
t	Thickness	1 mm
d	Load distribution distance	10 mm
f	Load amplitude	1400 N

Table 3: Parameters for the 2D portal frame problem.

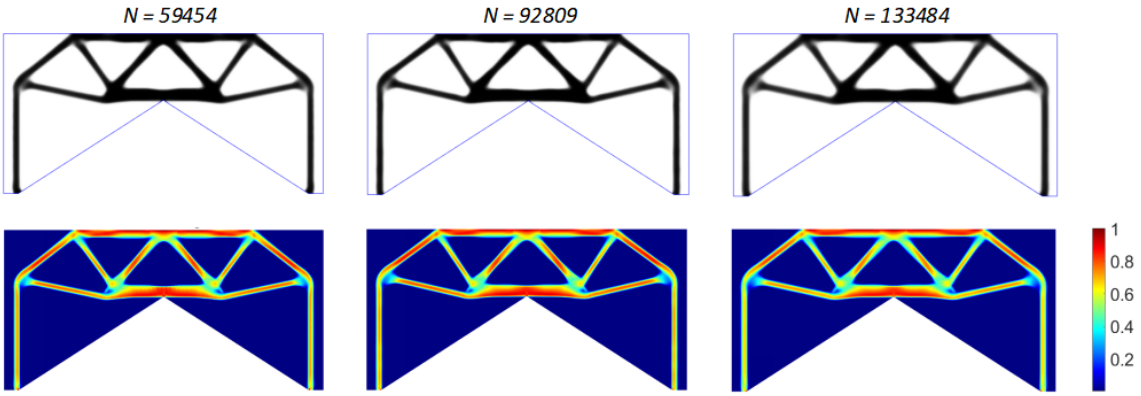

Figure 8: TO results and normalized constraint maps based on Sines fatigue constraints

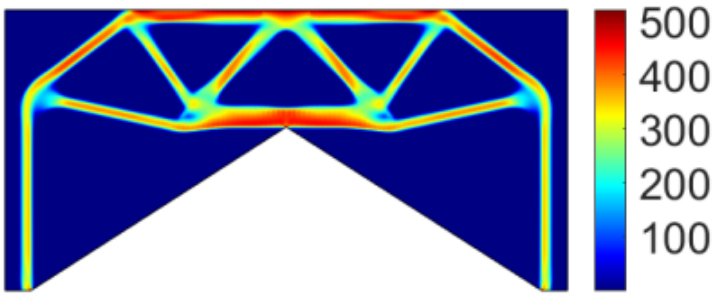

Figure 9: Von Mises stress map for 2D portal frame problem, unit: MPa

5 CONCLUSIONS

In this paper, a framework for TO considering Sines fatigue constraints is proposed. It combines the CNEM to solve the mechanical equilibrium and AL approach to solve the local minimum volume problem. Due to the nature of CNEM, the construction of the neighbor-based interpolation function is purely geometric and does not involve any artificially defined parameters. The AL method is able to significantly reduce the cost associated with a large number of constraints while providing a more consistent model than aggregation techniques. The stress-based Sines fatigue criteria is more conservative than the von Mises stress constraint. However, the fatigue criteria adopted in this paper cannot predict the direction of potential fatigue cracks, which will be the next step of this study.

REFERENCES

[1] M.P. Bendsøe, N. Kikuchi, Generating optimal topologies in structural design using a homogenization method. *Computer Methods in Applied Mechanics and Engineering*, **71**, 197–224, 1988.

[2] O. Sigmund, K. Maute, Topology optimization approaches. *Structural and Multidisciplinary Optimization*, **48**, 1031–1055, 2013.

[3] K. Sherif, W. Witteveen, K. Puchner, H.Irschik, Efficient topology optimization of large dynamic finite element systems using fatigue. *AIAA Journal*, **48**, 1339-1347, 2010.

[4] E. Holmberg, B. Torstenfelt, A. Klarbring, Fatigue constrained topology optimization. *Structural and Multidisciplinary Optimization*, **50**, 207-219, 2014.

[5] S.H. Jeong, D.H. Choi, G.H. Yoon, Fatigue and static failure considerations using a topology optimization method. *Applied Mathematical Modelling*, **39**, 1137-1162, 2015.

[6] J.W. Lee, G.H. Yoon, S.H. Jeong, Topology optimization considering fatigue life in the frequency domain. *Computers & Mathematics with Applications*, **70**, 1852-1877, 2015.

[7] M. Collet, M. Bruggi, M. Duysinx, Topology optimization for minimum weight with compliance and simplified nominal stress constraints for fatigue resistance. *Structural and Multidisciplinary Optimization*, **55**, 839-855, 2017.

[8] J. Oest, E. Lund, Topology optimization with finite-life fatigue constraints. *Structural and Multidisciplinary Optimization*, **56**, 1045-1059, 2017.

[9] S.L. Zhang, C. Le, A.L. Gain, J.A. Norato, Fatigue-based topology optimization with non-proportional loads. *Computer Methods in Applied Mechanics and Engineering*, **345**, 805-825, 2019.

[10] S. Suresh, S.B. Lindström, C.J. Thore, B. Torstenfelt, A. Klarbring, Topology optimization using a continuous-time high-cycle fatigue model. *Structural and Multidisciplinary Optimization*, **61**, 1011-1025, 2020.

[11] Z. Chen, K. Long, P. Wen, S. Nouman, Fatigue-resistance topology optimization of continuum structure by penalizing the cumulative fatigue damage. *Advances in Engineering Software*, **150**, 102924, 2020.

[12] K. Nabaki, J. Shen, X. Huang, Evolutionary topology optimization of continuum structures considering fatigue failure. *Materials and Design*, **166**, 107586, 2019.

[13] A. Diaz, O. Sigmund, Checkerboard patterns in layout optimization. *Structural and Multidisciplinary Optimization*, **10**, 40-45, 1995.

[14] C. Talischi, G.H. Paulino, C.H. Le, Honeycomb Wachspress finite elements for structural topology optimization. *Structural and Multidisciplinary Optimization*, **37**, 569-583, 2009.

[15] C. Talischi, G.H. Paulino, A. Pereira, I.F.M. Menezes, Polygonal finite elements for topology optimization: A unifying paradigm. *Structural and Multidisciplinary Optimization*, **82**, 671-698, 2010.

[16] C. Talischi, G.H. Paulino, A. Pereira, I.F.M. Menezes, A MATLAB implementation of a general topology optimization framework using unstructured polygonal finite element meshes. *Structural and Multidisciplinary Optimization*, **45**, 329-357, 2012.

[17] S. Li, S.N. Atluri, Topology-optimization of structures based on the MLPG mixed collocation method. *CMES - Computer Modeling in Engineering and Sciences*, **26**(1), 61-74, 2008.

[18] Z. Luo, N. Zhang, Y, Wang, W. Gao, Topology optimization of structures using meshless density variable approximants. *International Journal for Numerical Methods in Engineering*, **93**(4), 443-464, 2013.

[19] V. Shobeiri, Topology optimization using bi-directional evolutionary structural optimization based on the element-free Galerkin method. *Engineering Optimization*, **48**(3), 380-396, 2015.

[20] Z. Ullah, B. Ullah, W. Khan, Siraj-ul-Islam, Proportional topology optimisation with maximum entropy-based meshless method for minimum compliance and stress constrained problems. *Engineering with Computers*, **38**, 5541-5561, 2022.

[21] Y.D. Chen, E. Monteiro, I. Koutiri, V. Favier, Topology optimization using the constrained natural element method. *ASMO-UK 12 / ASMO-Europe 1 / ISSMO Conference on Engineering Design Optimization*, University of Leeds, England, 17-18 July, 2022.

[22] J. Braun, M. Sambridge, A numerical method for solving partial differential equations on highly irregular evolving grids. *Nature*, **376**, 655-660, 1995.

[23] N. Sukumar, B. Moran, T. Belytschko, The natural element method in solid mechanics. *International Journal for Numerical Methods in Engineering*, **43**, 839-887, 1998.

[24] J. Yvonnet, D. Ryckelynck, P. Lorong, F. Chinesta, A new extension of the natural element method for non-convex and discontnuous problems: the constrained natural element method. *International Journal for Numerical Methods in Enginering*, **60**, 1451-1474, 2004.

[25] L. Illoul, P. Lorong, On some aspects of the CNEM implementation in 3D in order to simulate high speed machining or shearing. *Computers and Structures*, **89**(11-12), 940-958, 2011.

[26] R. Sibson, A brief description of natural neighbor interpolation. *Interpreting Multivariate Data*, John Wiley & Sons, New York, 21-36, 1981.

[27] J.S. Chen, C.T. Wu, S. Yoon, Y. You, A stabilized conforming nodal integration for Galerkin mesh-free methods. *International Journal for Numerical Methods in Engineering*, **50**, 435-466, 2001.

[28] T. Zegard, G.H. Paulino, Bridging topology optimization and additive manufacturing. *Structural and Multidisciplinary Optimization*, **53**, 175–192, 2016.

[29] F. Wang, B.S. Lazarov, O. Sigmund, On projection methods, convergence and robust formulations in topology optimization. *Structural and Multidisciplinary Optimization*, **43**(6), 767–784, 2011.

[30] G. Sines, Metal Fatigue. *McGraw Hill, New York*, 145-169, 1959.

[31] F.V. Senhora, O. Giraldo-Londoño, I.F.M. Menezes, G.H. Paulino, Topology optimization with local stress constraints: a stress aggregation-free approach. *Structural and Multidisciplinary Optimization*, **62**, 1639–1668, 2020.

[32] T.M. Mower, M.J. Long, Mechanical behavior of additive manufactured, powder-bed laser-fused materials. *Materials Science & Engineering A*, **651**, 198–213, 2016.

[33] A. Fatemi, R. Molaei, S. Sharifimehr, N. Phan, N. Nima Shamsaei, Multiaxial fatigue behavior of wrought and additive manufactured Ti-6Al-4V including surface finish effect. *International Journal of Fatigue*, **100**, 347–366, 2017.